

JES

JOURNAL OF
ENVIRONMENTAL
SCIENCES

ISSN 1001-6742
CN 11-2629X

March 1, 2014 Volume 26 Number 3
www.jesc.ac.cn

Unexpected malformations in
Xenopus tropicalis



Sponsored by
Research Center for Eco-Environmental Sciences
Chinese Academy of Sciences

CONTENTS

Aquatic environment

- Metal composition of layered double hydroxides (LDHs) regulating ClO_4^- adsorption to calcined LDHs via the memory effect and hydrogen bonding
Yajie Lin, Qile Fang, Baoliang Chen 493
- Limitation of spatial distribution of ammonia-oxidizing microorganisms in the Haihe River, China, by heavy metals
Chao Wang, Baoqing Shan, Hong Zhang, Yu Zhao 502
- Temperature sensitivity of organic compound destruction in SCWO process
Yaqin Tan, Zheming Shen, Weimin Guo, Chuang Ouyang, Jinping Jia, Weili Jiang, Haiyun Zhou 512
- Influence of moderate pre-oxidation treatment on the physical, chemical and phosphate adsorption properties of iron-containing activated carbon
Zhengfang Wang, Mo Shi, Jihua Li, Zheng Zheng 519
- Reduction of DOM fractions and their trihalomethane formation potential in surface river water by in-line coagulation with ceramic membrane filtration
Pharkphum Rakruam, Suraphong Wattanachira 529
- N_2O emission from nitrogen removal via nitrite inoxic-anoxic granular sludge sequencing batch reactor
Hong Liang, Jiaoling Yang, Dawen Gao 537
- Influence of stabilizers on the antimicrobial properties of silver nanoparticles introduced into natural water
Aleksandra Burkowska-But, Grzegorz Sionkowski, Maciej Walczak 542
- Addition of hydrogen peroxide for the simultaneous control of bromate and odor during advanced drinking water treatment using ozone
Yongjing Wang, Jianwei Yu, Dong Zhang, Min Yang 550
- Nitric oxide removal by wastewater bacteria in a biotrickling filter
Hejingying Niu, Dennis Y C Leung, Chifang Wong, Tong Zhang, Mayngor Chan, Fred C C Leung 555
- Elucidating the removal mechanism of *N,N*-dimethyldithiocarbamate in an anaerobic-anoxic-oxic activated sludge system
Yongmei Li, Xianzhong Cao, Lin Wang 566
- Influencing factors of disinfection byproducts formation during chloramination of Cyclops metabolite solutions
Xingbin Sun, Lei Sun, Ying Lu, Jing Zhang, Kejing Wang 575

Atmospheric environment

- Sources of nitrous and nitric oxides in paddy soils: Nitrification and denitrification
Ting Lan, Yong Han, Marco Roelcke, Rolf Nieder, Zucong Cai 581
- Upper Yellow River air concentrations of organochlorine pesticides estimated from tree bark, and their relationship with socioeconomic indices
Chang He, Jun Jin, Bailin Xiang, Ying Wang, Zhaohui Ma 593
- Mechanism and kinetic properties of NO_3^- -initiated atmospheric degradation of DDT
Cai Liu, Shanqing Li, Rui Gao, Juan Dang, Wenxing Wang, Qingzhu Zhang 601
- Sorption and phase distribution of ethanol and butanol blended gasoline vapours in the vadose zone after release
Ejike Ugwoha, John M. Andresen 608

Terrestrial environment

- Effects of temperature change and tree species composition on N_2O and NO emissions in acidic forest soils of subtropical China
Yi Cheng, Jing Wang, Shenqiang Wang, Zucong Cai, Lei Wang 617

Environmental biology

- Influence of sunlight on the proliferation of cyanobacterial blooms and its potential applications in Lake Taihu, China
Qichao Zhou, Wei Chen, Kun Shan, Lingling Zheng, Lirong Song 626
- Bioavailability and tissue distribution of Dechloranes in wild frogs (*Rana limnocharis*) from an e-waste recycling area in Southeast China
Long Li, Wenyue Wang, Quanxia Lv, Yujie Ben, Xinghong Li 636

Environmental health and toxicology

- Unexpected phenotypes of malformations induced in *Xenopus tropicalis* embryos by combined exposure to triphenyltin and 9-*cis*-retinoic acid
Jingmin Zhu, Lin Yu, Lijiao Wu, Lingling Hu, Huahong Shi 643
- Expression of sulfur uptake assimilation-related genes in response to cadmium, bensulfuron-methyl and their co-contamination in rice roots
Jian Zhou, Zegang Wang, Zhiwei Huang, Chao Lu, Zhuo Han, Jianfeng Zhang, Huimin Jiang, Cailin Ge, Juncheng Yang 650

Environmental catalysis and materials

Reaction mechanism and metal ion transformation in photocatalytic ozonation of phenol and oxalic acid with Ag^+/TiO_2 Yingying Chen, Yongbing Xie, Jun Yang, Hongbin Cao, Yi Zhang	662
Effect of TiO_2 calcination temperature on the photocatalytic oxidation of gaseous NH_3 Hongmin Wu, Jinzhu Ma, Changbin Zhang, Hong He	673
Effects of synthesis methods on the performance of Pt + Rh/ $\text{Ce}_{0.6}\text{Zr}_{0.4}\text{O}_2$ three-way catalysts Zongcheng Zhan, Liyun Song, Xiaojun Liu, Jiao Jiao, Jinzhou Li, Hong He	683
Catalytic combustion of soot over ceria-zinc mixed oxides catalysts supported onto cordierite Leandro Fontanetti Nascimento, Renata Figueredo Martins, Rodrigo Ferreira Silva, Osvaldo Antonio Serra	694
Effects of metal and acidic sites on the reaction by-products of butyl acetate oxidation over palladium-based catalysts Lin Yue, Chi He, Zhengping Hao, Shunbing Wang, Hailin Wang	702
Mechanism of enhanced removal of quinonic intermediates during electrochemical oxidation of Orange II under ultraviolet irradiation Fazhan Li, Guoting Li, Xiwang Zhang	708

Serial parameter: CN 11-2629/X*1989*m*223*en*P*26*2014-3

Available online at www.sciencedirect.com

Journal of Environmental Sciences

www.jesc.ac.cn

Effect of TiO₂ calcination temperature on the photocatalytic oxidation of gaseous NH₃

Hongmin Wu, Jinzhu Ma, Changbin Zhang*, Hong He

Research Center for Eco-Environmental Sciences, Chinese Academy of Sciences, Beijing 100085, China. E-mail: hmwu_st@rcees.ac.cn

ARTICLE INFO

Article history:

Received 13 April 2013

revised 27 May 2013

accepted 29 May 2013

Keywords:

photocatalysis

NH₃TiO₂

calcination temperature

indoor air quality

DOI: 10.1016/S1001-0742(13)60441-6

ABSTRACT

Carbon-modified titanium dioxide (TiO₂) was prepared by a sol-gel method using tetrabutyl titanate as precursor, with calcination at various temperatures, and tested for the photocatalytic oxidation (PCO) of gaseous NH₃ under visible and UV light. The test results showed that no samples had visible light activity, while the TiO₂ calcined at 400°C had the best UV light activity among the series of catalysts, and was even much better than the commercial catalyst P25. The catalysts were then characterized by X-ray diffractometry, Brunauer-Emmett-Teller adsorption analysis, Raman spectroscopy, thermogravimetry/differential scanning calorimetry coupled with mass spectrometry, ultraviolet-visible diffuse reflectance spectra, photoluminescence spectroscopy and *in situ* diffuse reflectance infrared Fourier transform spectroscopy. It was shown that the carbon species residuals on the catalyst surfaces induced the visible light adsorption of the samples calcined in the low temperature range (< 300°C). However, the surface acid sites played a determining role in the PCO of NH₃ under visible and UV light over the series of catalysts. Although the samples calcined at low temperatures had very high SSA, good crystallinity, strong visible light absorption and also low PL emission intensity, they showed very low PCO activity due to their very low number of acid sites for NH₃ adsorption and activation. The TiO₂ sample calcined at 400°C contained the highest number of acid sites among the series of catalysts, therefore showing the highest performance for the PCO of NH₃ under UV light.

Introduction

Indoor air quality has recently attracted more and more attention with the increasing concern for the public environment and health, especially in urban cities (Fischer et al., 2003). Gaseous ammonia (NH₃), released from walls containing urea or ammonia compound-based antifreezes, is becoming one of the major indoor air pollutants, particularly in China (Bai et al., 2006; Meng et al., 2011). NH₃ is an alkaline gas with a pungent odor and is harmful to the environment and people's health. Long-time exposure to NH₃ can cause irritation of the skin, throat, lungs and eyes, affect the respiratory system and even cause permanent

damage to the organs (Bai et al., 2006). Therefore, it is of great interest to eliminate indoor air NH₃ to meet environmental regulations and health needs.

The traditional remediation techniques, such as adsorption and ventilation, cannot eliminate NH₃ completely (Kim and Shin, 2001). NH₃ can be completely removed by selective catalytic oxidation using various catalysts such as metals, metal oxides and zeolites, but they cannot realize effective abatement of gaseous NH₃ at room temperature (Akah et al., 2005; Zhang et al., 2009; Cui et al., 2010). Photocatalytic oxidation (PCO) is a promising method for removing indoor air pollutants such as formaldehyde, volatile organic compounds, etc, under ultraviolet (UV) light irradiation at ambient temperature (Guo et al., 2008; Chen et al., 2009; Mo et al., 2009). TiO₂ is a very effective photocatalyst known for the stability of its chemical struc-

* Corresponding author. E-mail: cbzhang@rcees.ac.cn

ture, biocompatibility and physical, optical and electrical properties (Chen and Mao, 2007). Therefore, TiO₂-based photocatalysts have been extensively studied for the elimination of indoor and outdoor organic pollutants from both water and air in various environmental applications (Carp, 2004; Fu et al., 2005; Li et al., 2010; Liu et al., 2012). In contrast, only a relative few recent studies have been focused on the photocatalytic removal of gaseous NH₃. Several types of modified TiO₂-based photocatalysts such as TiO₂-activated carbon composites (Nazir et al., 2003; Hou et al., 2006), woven fabric-supported TiO₂ (Dong et al., 2007a, 2007b) and latex paint-supported film nano-TiO₂ (Geng et al., 2008a, 2008b), etc, have been evaluated for the PCO of NH₃ under UV light irradiation. The products distribution during the PCO of NH₃ has been investigated by FT-IR or GC/GC-MS, and N₂ was found to be the main gaseous product; N₂O, NO₂⁻ and NO₃⁻ were registered as the major by-products (Hou et al., 2006; Yamazoe et al., 2007a; Yamazoe et al., 2007b; Kolinko and Kozlov, 2009).

The previous studies on the PCO of NH₃ were all performed under UV light irradiation. Therefore, the development of visible-light-activated TiO₂ for the PCO of NH₃ is still of great interest. Most attempts to realize visible-light-activation of TiO₂ have been concentrated on doping TiO₂ with nonmetallic elements such as carbon (Ren et al., 2007; Huang et al., 2008; Dong et al., 2011), nitrogen (Kuroda et al., 2005; Kang et al., 2008; Cheng et al., 2012), sulfur (Jimmy et al., 2005; Li et al., 2007), fluorine (Yu et al., 2002; Wang et al., 2008; Li and Shang, 2010), iodine (Tojo et al., 2008) and boron (In et al., 2007). In particular, carbon atom-doping has been shown to be more effective than other materials in promoting the visible light activation of TiO₂ (Leary and Westwood, 2011). Several methods such as impregnation (Miyawaki et al., 2011), mild oxidation of TiC (Shen et al., 2006), sol-gel (Lin et al., 2006; Xiao and Ouyang, 2009), hydrothermal synthesis (Dong et al., 2009), chemical vapor deposition (Kuo et al., 2007), etc, have been employed to synthesize carbon-doped TiO₂. Among them, the sol-gel technique, which is able to achieve intimate mixing and chemical interaction between carbon and TiO₂ at relatively low temperatures, is the most widely applied method (Macwan et al., 2011). In some cases, the source of carbon species was from the organic precursor of TiO₂ and the optimum carbon doping amount could be tuned by changing the calcination temperature, therefore the calcination temperature showed a great influence on the activity of these photocatalysts (Lin et al., 2006; Górska et al., 2008; Xiao and Ouyang, 2009). Tseng et al. (2006) prepared carbon-modified catalysts for PCO of NO_x by a sol-gel process using titanium alkoxides and ethanol with nitric acid at various calcination temperatures (150–600°C). They found that the presence of carbonaceous species was responsible for the absorption of visible light by TiO₂, and a sample

calcined at 200°C exhibited the highest photoactivity for NO oxidation under both visible and UV light. Górska et al. (2008) prepared carbon-modified catalysts using titanium(IV) isopropoxide and studied the effect of calcination temperature on TiO₂ photoactivity in phenol degradation under visible and UV light. They observed that a sample calcined at 350°C was the most visible-light-active catalyst and that the carbon residues formed during calcination accounted for the visible light activation.

In this study, we also prepared carbon-containing nano-sized TiO₂ catalysts with the method described by Tseng et al. (2006). Our attempt here was aimed toward screening for a visible-light-active photocatalyst for the PCO of gaseous NH₃ by tuning the calcination temperature during preparation. The as-prepared catalysts were tested under both visible and UV light. Although the series of catalysts was reported to be visible-light-active for NO oxidation (Tseng et al., 2006), these catalysts showed no visible-light activity for the PCO of gaseous NH₃. In addition, the sample calcined at 400°C, rather than the sample calcinated at 200°C, exhibited the highest UV light activity for NH₃ oxidation. The influence of calcination temperature on the specific surface area (SSA), crystallinity, optical properties, carbon species residual and also the acidity of the samples was studied using XRD, Raman, BET, TG-DSC, MS, UV-Vis, PL, and *in situ* DRIFTS methods. The relationship between the physical and chemical properties of samples and their photoactivities was carefully examined.

1 Experiment section

1.1 Catalyst preparation

TiO₂ was prepared by HNO₃ (AR) catalyzed hydrolysis of tetrabutyl titanate (Ti(OC₄H₉)₄, CP) followed by calcination at different temperatures. Typically, 17 g tetrabutyl titanate was first added dropwise into 90 mL of anhydrous ethanol and 20 mL of deionized water under magnetic stirring. Then, 4 mL of 1 mol/L HNO₃ was added dropwise into the mixture. A white precipitate was formed after the mixed solution was uniformly stirred at 25°C for 3 hr, which was filtered, washed and then dried at 110°C overnight. The dried powder was crushed and calcined in air at different controlled temperatures (150°C, 200°C, 300°C, 400°C, 500°C, 600°C for 5 hr. For simplicity, the final catalysts are labeled as T_x, where *x* represents the calcination temperature.

1.2 Characterization of catalysts

Powder X-ray diffraction (XRD) measurements of the catalysts were carried out on a PANalytical X'Pert Pro diffractometer using Cu K α radiation ($\lambda = 0.154056$ nm) operating at 40 kV and 40 mA. The patterns were

taken over the 2θ range from 10 to 90° with a step size of 0.026° . Nitrogen adsorption-desorption isotherms were obtained at -196°C using a Quantasorb-18 automatic instrument (Quanta Chrome Instrument Co., USA). Raman spectra were recorded on a UV resonance Raman spectrometer (UVR DLPC-DL-03). The laser excitation was 325 nm and the laser power was 40 mW. High-resolution transmission electron microscopy (HRTEM) images were obtained on a JEM-2010 electron microscope (JEOL, Japan). TG-DSC was conducted on a METTLER TOLEDO apparatus to characterize the weight change and endothermic-exothermic status of the TiO_2 catalysts. A quadrupole mass spectrometer (MS) was used to record the signals of H_2O ($m/z = 18$) and CO_2 ($m/z = 44$) evolved during the heating process.

Diffuse-reflectance UV-Vis spectra were obtained under ambient conditions on a UV-1700 (Shimadzu, Japan) spectrometer. The range was 190–800 nm and the scan rate was 120 nm/min. Photoluminescence (PL) spectra were measured at room temperature on a fluorescence spectrophotometer (F-4500, Hitachi, Japan). The exciting wavelength was 300 nm; the scanning speed was 240 nm/min and the PMT voltage was 400 V. The widths of the excitation and emission slits were 5.0 nm. *In situ* DRIFTS of NH_3 adsorption were performed on an FT-IR spectrometer (Nicolet Nexus 670) equipped with a Smart Collector and an MCT detector. The sample was first pretreated at the calcination temperature in a flow of 20 vol% O_2/N_2 for 30 min and then cooled to 25°C . The samples were exposed to 695 mg/m^3 NH_3/N_2 at a flow of 200 mL/min for 1 hr and then purged by N_2 for 1 hr.

1.3 Catalytic evaluation of materials

The PCO of NH_3 was carried out in a continuous flow system. All reactions were performed in a black-colored box with a 500-W ultraviolet high pressure mercury lamp. The intensity of the UV light irradiation with the peak wavelength at 365 nm on the catalysts' surface was 0.46 mW/cm^2 . There was a fan above the lamp and circulated

cooling water under the vessel to control the reaction temperature at 24°C . 50 mg catalyst was first dispersed in water and then the turbid solution was spread over a round stainless steel sample dish with diameter of 5.5 cm. The sample dish was held at 60°C to fully remove water and then cooled down to room temperature before use. The reactant gas was 35 mg/m^3 NH_3 , 20 vol% O_2 , and balance N_2 with a total flow rate of 200 mL/min, and the relative humidity was 50%. The inlet and outlet gases were monitored by an FT-IR spectrometer (Nicolet 380) equipped with a 2 m path length gas cell.

2 Results and discussion

2.1 BET, phase structure and morphology

Nitrogen adsorption-desorption isotherms were measured to determine the textural structures of TiO_2 samples calcined at various temperatures and the results are shown in **Table 1**. It is clear that the calcination temperature had a big influence on the textural structures. Without calcination, the sample had a SSA of $236.8\text{ m}^2/\text{g}$. With calcination at 150 and 200°C , the SSA was slightly enhanced and the T_{200} sample presented the highest SSA ($282.7\text{ m}^2/\text{g}$) among this series of catalysts. However, further increasing the temperature resulted in a dramatic decrease of SSA and the T_{600} sample exhibited extremely low SSA ($3.0\text{ m}^2/\text{g}$). The structural parameters of P25 are also presented for comparison.

XRD patterns of TiO_2 catalysts calcined at various temperatures were then measured to characterize the bulk crystalline structures of the TiO_2 samples and the results are shown in **Fig. 1**. When the calcination temperatures were not higher than 400°C , anatase was the main phase, with peaks at $2\theta = 25.3^\circ(101)$, $37.8^\circ(004)$, $48.1^\circ(200)$, $54.0^\circ(105)$ and $55.1^\circ(211)$ (JCPDS no. 21-1272). A small brookite phase peak at $2\theta = 30.8^\circ(121)$ was also observed

Table 1 Structural parameters of the TiO_2 samples calcined at various temperatures and the weight losses during the TG experiments

Sample	SSA (m^2/g)	Pore diameter (nm)	Pore volume (cc/g)	Crystal size (nm)	Weight loss 35– 125°C	Weight loss 125– 500°C
Uncalcined	236.8	3.48	0.21	7.8 ^a	1.47% ^h	14.22% ^{h+c}
T_{150}	245.3	3.56	0.22	8.4 ^a	1.43% ^h	11.57% ^{h+c}
T_{200}	282.7	3.61	0.25	8.2 ^a	1.59% ^h	10.52% ^{h+c}
T_{300}	243.5	4.01	0.24	8.5 ^a	1.40% ^h	5.46% ^{h+c}
T_{400}	145.2	5.39	0.2	9.3 ^a	0.90% ^h	2.33% ^h
T_{500}	58.6	6.81	0.1	16.7 ^a 35.6 ^b	0.83% ^h	1.30% ^h
T_{600}	3.0	9.25	0.01	53.7 ^b	0.17% ^h	0
P25	59.1	11.8	0.17	20.8 ^a 30.7 ^b	/	/

^a represents the size of anatase phase; ^b represents the size of rutile phase. ^h represents the water desorbed during the TG process; ^c represents the carbon species lost during the TG process.

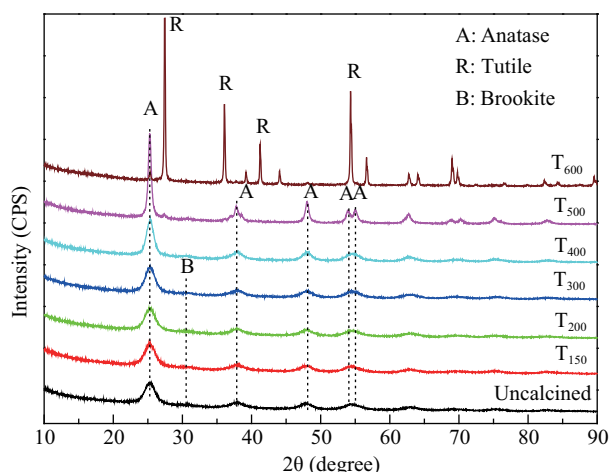


Fig. 1 XRD patterns of the TiO₂ catalysts calcined at various temperatures.

(JCPDS no. 29-1360) in these samples. The phase transformation of TiO₂ was observed at 500°C. The rutile phase appeared in the T₅₀₀ sample and became the dominant phase in the T₆₀₀ sample with peaks at $2\theta = 27.4^\circ(110)$, $36.1^\circ(101)$, $41.2^\circ(111)$, $54.3^\circ(211)$ (JCPDS no. 21-1276). The rutile phase of TiO₂ is normally formed above 600°C with complete transformation to rutile phase at 800°C (Porter et al., 1999). The present XRD patterns show that the phase transformation of the synthesized TiO₂ occurred at 500°C and was almost finished at 600°C, which was possibly caused by the carbon impurities introduced from the alkoxide group of the TiO₂ precursor (Figs. 4 and 5) (Lettmann et al., 2001).

The crystal sizes of TiO₂ were calculated from the half-width of peaks using Scherrer's equation ($d = 0.9\lambda/\beta \cdot \cos\theta$). The size of the anatase phase was calculated from the peak at $2\theta = 25.3^\circ$ and the size of the rutile phase was calculated from the peak at $2\theta = 27.4^\circ$, and the data are presented in **Table 1**. When the calcination temperature was not higher than 300°C, the calcination showed little influence on the anatase crystal size. The uncalcined, T₁₅₀, T₂₀₀, and T₃₀₀ samples all presented very similar crystal sizes of around 8 nm. The calcination at 400°C resulted in a slight increase of the anatase crystal size to 9.3 nm. In contrast, calcination at 500 and 600°C dramatically increased the crystalline sizes of both the anatase and rutile phase. The T₅₀₀ sample exhibited the anatase crystal size of 16.7 nm with rutile crystal size of 35.6 nm, and the T₆₀₀ sample showed the rutile crystal size of 53.7 nm. The present results are in good agreement with the reported measurements (Tseng et al., 2006).

Raman spectra were measured to examine the surface structure of TiO₂ samples and the results are shown in **Fig. 2**. The commercial anatase TiO₂ was first measured as a reference, and four characteristic peaks were observed at around 146, 402, 521 and 636 cm⁻¹ (Balachandran and Eror, 1982). The uncalcined sample showed the typical spectrum of anatase phase TiO₂ with a slight red shift

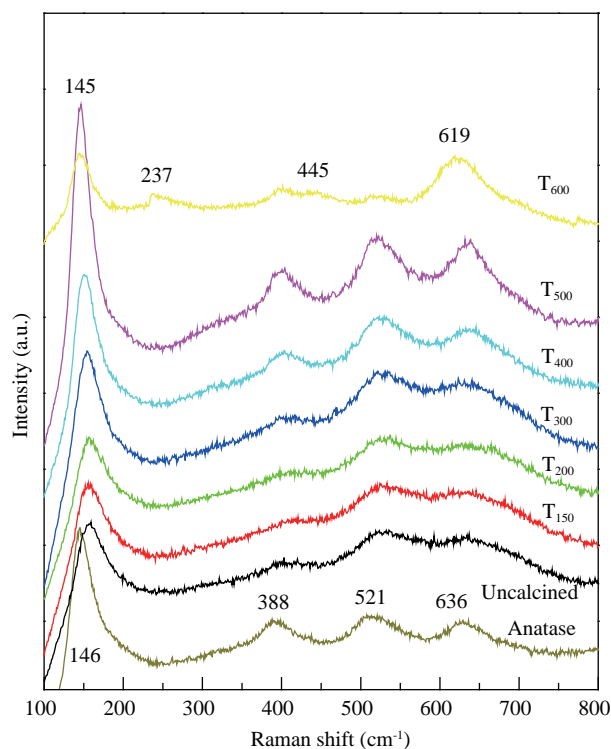


Fig. 2 Raman spectra of catalysts prepared at various temperatures.

and low peak intensities. When the catalysts were calcined at 150, 200 and 300°C, the Raman features of the TiO₂ samples are almost identical to that of the uncalcined one. T₄₀₀ and T₅₀₀ samples still showed spectra similar to anatase phase TiO₂ but with increased peak intensities, possibly due to the increase of the particle size during high temperature calcination (Xue et al., 2012). In contrast, the anatase peaks in the T₆₀₀ sample sharply decreased and the rutile peaks at 237, 445 and 619 cm⁻¹ became dominant in the spectrum (Balachandran and Eror, 1982).

HR-TEM images of the uncalcined, T₂₀₀ and T₄₀₀ samples were measured to examine the morphologies and the images are shown in **Fig. 3**. The images indicated that the catalysts consist of large numbers of particulates with a size of around 10 nm. The particle size of the uncalcined sample was similar to that of the T₂₀₀ samples. In contrast, T₄₀₀ showed a slight larger particle size than the T₂₀₀ samples due to the high temperature calcination, which is consistent with the results of XRD. The three catalysts all showed the same lattice spacing (0.35 nm), indicating that all the catalysts showed exposure of {101} facets and the calcination temperature did not induce change of the crystal lattice and crystal facets. Moreover, no obvious differences in the crystal parameters were observed among these three catalysts.

2.2 TG-DSC-MS

TG-DSC analysis was performed to characterize the phase transition of TiO₂ and the amounts of impurities on the catalyst surfaces. **Figure 4** depicts the TG and DSC

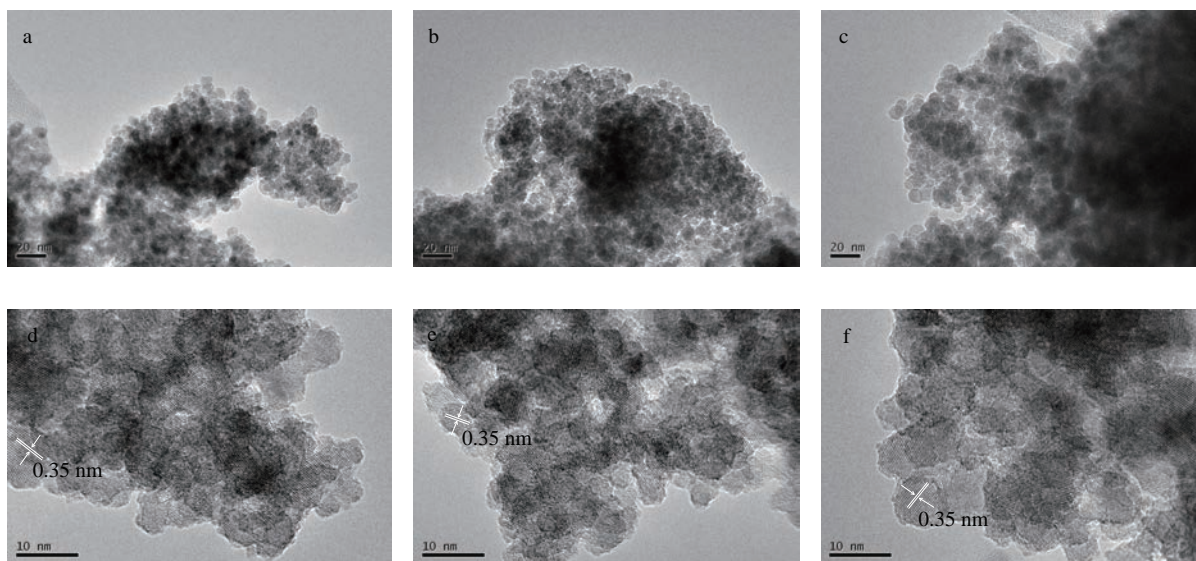


Fig. 3 HR-TEM images of the uncalcined (a, d), T₂₀₀ (b, e) and T₄₀₀ (c, f) samples.

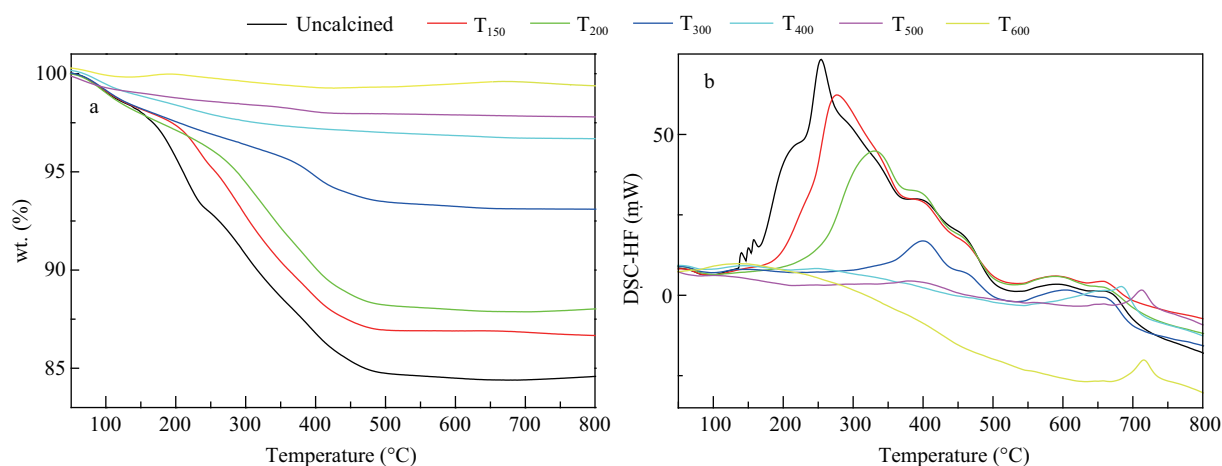


Fig. 4 TG (a) and DSC (b) curves of the catalysts calcined at various temperatures.

curves of the catalysts during heating in air. All the samples showed small weight loss peaks from 35 to 125°C. When the temperature was further increased from 125°C to 500°C, substantial weight losses were observed (Fig. 4a) accompanied with clear exothermic peaks for the uncalcined, T₁₅₀, T₂₀₀, and T₃₀₀ samples (Fig. 4b). In contrast, T₄₀₀, T₅₀₀, and T₆₀₀ samples presented much lower weight loss. In addition, there were small exothermic peaks between 500 and 750°C in all samples, indicating the anatase-rutile transformation in this temperature range. The effluent gases were monitored by MS during the TG analysis and the MS results are shown in Fig. 5. Only water was detected between 35 and 125°C, confirming that the small weight loss was due to desorption of physisorbed water molecules. In addition, CO₂ and H₂O signals simultaneously appeared between 125 and 500°C in the catalysts calcined at temperatures lower than 400°C, indicating that the impurities were mainly carbon species introduced from

the precursor tetrabutyl titanate. In contrast, no CO₂ signal appeared for T₄₀₀, T₅₀₀ and T₆₀₀ samples, showing that there was no carbon species left when the catalysts were calcined above 400°C. The weight losses were roughly calculated based on the TG results and the results are also presented in Table 1. It is clear that the weight loss decreased with the increase of the calcination temperature.

2.3 UV-Vis analysis

The TiO₂ band gap plays an important role in the photocatalytic performance (Yu et al., 2007; He et al., 2011). UV-Vis diffuse reflectance spectra were next measured to investigate the optical properties of TiO₂ prepared at various temperatures and Fig. 6a gives the light absorbance spectra. The uncalcined sample showed a slight absorption in the visible light region above 400 nm. Annealing at 150 and 200°C dramatically enhanced the visible light absorption of T₁₅₀ and T₂₀₀, which should be ascribed to the

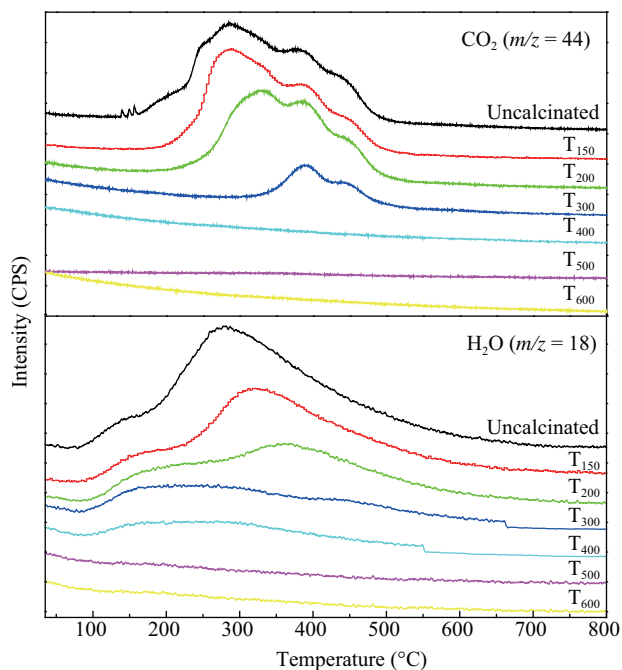


Fig. 5 MS spectra of the catalysts calcined at various temperatures during the TG analysis.

presence of residual carbonaceous species on the catalyst surfaces (Tseng et al., 2006). However, further increasing the calcination temperature to 300 and 400°C decreased the visible light absorption. The T_{300} sample presented a much lower intensity of visible light absorption and the T_{400} sample showed no response to visible light due to the gradual removal of carbonaceous species with high-temperature annealing. As the calcination temperatures were further increased to 500 and 600°, the samples responded to the visible light again, which is attributed to the appearance of rutile phase TiO_2 (Hoffmann et al., 1995; Góska et al., 2008; Wang et al., 2012). The plots of the transformed Kubelka-Munk functions as a function of light energy are shown in **Fig. 6b** and the inset shows the

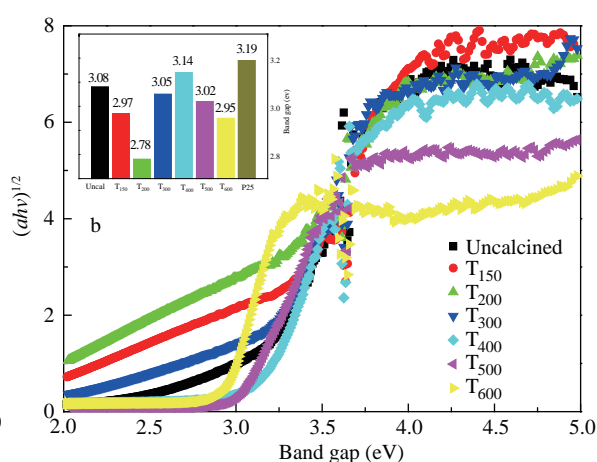
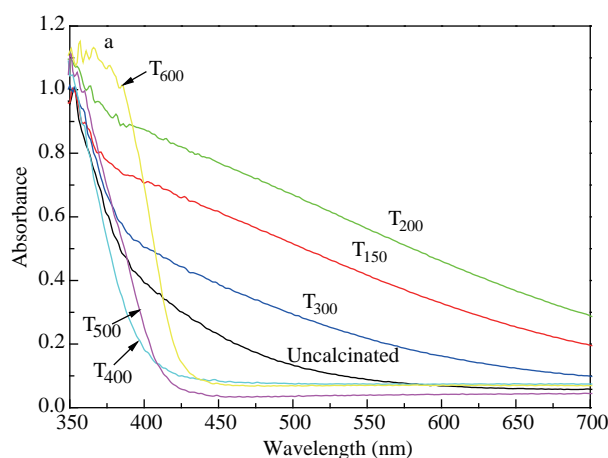


Fig. 6 (a) UV-Vis diffuse reflection spectra and (b) the plots of transformed Kubelka-Munk function versus the energy of light of the catalysts calcined at different temperatures (inset is the band gap calculated).

band gap energies of the catalysts roughly calculated based on the plots. Among the series of catalysts, the T_{200} sample showed the lowest band-gap energy of 2.78 eV, while the T_{400} presented the highest band-gap energy of 3.14 eV, similar to that of the commercial catalyst P25 (3.19 eV).

2.4 Photoluminescence analysis

Photoluminescence (PL) spectra of catalysts calcined at various temperatures were next measured to investigate the efficiency of charge carrier trapping, migration, transferring and the separation of photogenerated electron-hole pairs (Shi et al., 2007). A weaker PL emission signal is commonly indicative of higher photocatalytic activity (Chen et al., 2008; He et al., 2011). As depicted in **Fig. 7**, several emission bands were observed in the PL spectra. The broad emission band at around 400 nm is attributed to the emission of the band gap transition (Lü et al., 2012). The other five peaks ranging from 440 nm to 500 nm are due to surface oxygen vacancies, impurities and defects (Yu et al., 2011). Overall, the sequence of the PL intensities was in the order of $\text{P25} > T_{600} > T_{500} > T_{400} > T_{300} > T_{150} > T_{200}$. The commercial P25 showed the highest PL intensity among all samples. The carbon-free samples (T_{400} , T_{500} and T_{600}) demonstrated slightly lower PL signals than that of the commercial P25. In contrast, the carbon-containing samples (T_{150} , T_{200} and T_{300}) presented very low emission intensities and T_{200} showed the lowest signal, indicating that the residual carbon species significantly reduced the recombination rate of the photo-induced electrons and holes in the catalysts (Yu et al., 2011).

2.5 Activity test

The prepared catalysts were first evaluated for the PCO of NH_3 under visible light. All as-prepared samples showed no measurable activity for the photocatalytic oxidation of gaseous NH_3 . The catalysts were then tested under UV light (365 nm). **Figure 8a** presents the NH_3 conversion under UV light with time on-stream over all catalysts.

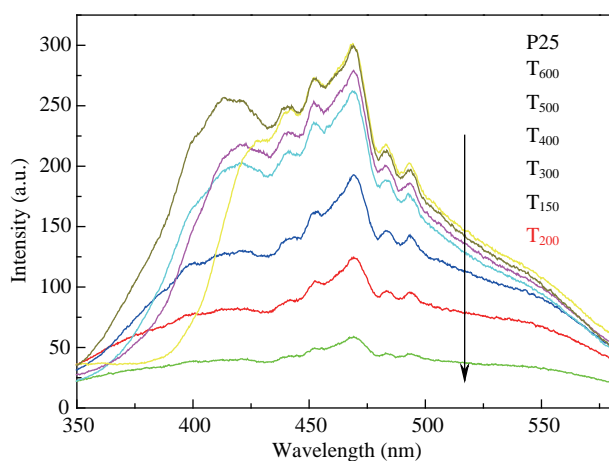


Fig. 7 Photoluminescence spectra of the catalysts calcined at various temperatures.

The calcination temperature showed a big influence on the activity. The photoactivity of TiO_2 calcined at various temperatures was in the order of: $T_{400} > \text{P25} > T_{500} > T_{300} > T_{200} > T_{150} > T_{600}$. The T_{150} and T_{200} samples showed very poor activity and only about 7% NH_3 conversion was obtained. Increasing the calcination to 300°C enhanced the NH_3 conversion to about 15%. T_{400} presented the highest NH_3 conversion (about 43%) among the catalysts. Further increasing the calcination temperature to 500°C and 600°C resulted in a significant drop in NH_3 conversion. In order to clearly show the influence of calcination temperature on activity, NH_3 conversions at 2 hr reaction time were selected and compared with each other in **Fig. 8b**. It is clear that T_{400} exhibits the best photocatalytic activity, even much better than commercial P25.

The photoactivity of TiO_2 was reported to be closely related to a combination of factors such as the SSA, pore volume, crystallinity, band gap energy and also the electron-hole recombination, etc. (Zhang et al., 2000). In the series of samples, the carbon-containing samples (T_{150} ,

T_{200} and T_{300}), especially the T_{200} sample, showed very high SSA (**Table 1**), good crystallinity (**Fig. 1**), strong visible light absorption (**Fig. 6a**), low band-gap energy (**Fig. 6b**) and also low recombination rate of electron and hole pairs (**Fig. 7**), therefore these catalysts should have high visible light activity for NH_3 oxidation. Previously, T_{150} , T_{200} and T_{300} samples (prepared by the same method) have demonstrated high activity for NO oxidation under visible-light illumination and the T_{200} sample was the best one (Tseng et al., 2006). However, in this study, the carbon-containing samples showed no visible light activity for the PCO of NH_3 . In addition, as shown in **Fig. 8**, these samples also showed very low activities under UV-light irradiation. In contrast, although T_{400} , which is a carbon-free sample with moderate SSA, the widest band gap (3.14 eV) and also high PL intensity, was not active under visible-light, it however demonstrated the highest NH_3 removal performance under UV-light among the series of catalysts. Therefore, the above-mentioned factors such as SSA, band gap and electron-hole recombination, etc., played no determining role in the photocatalytic oxidation of gaseous NH_3 over these catalysts. There must be another more important factor affecting the PCO of NH_3 .

2.6 In situ DRIFTS

Surface acidity is one of the factors which influence the photoactivity of TiO_2 (Choi et al., 2007; Yamazoe et al., 2007a). Since NH_3 is an alkaline gas, the surface acidity of the catalyst should have much more effect on the PCO of NH_3 than of an acidic gas such as NO. Therefore, *in situ* DRIFTS analyses of NH_3 -adsorbed catalysts were further carried out to probe the nature of the Lewis and Brønsted acid sites. **Figure 9** shows the *in situ* DRIFTS spectra of NH_3 adsorption over the series of catalysts. The spectra displayed NH_3 adsorption bands at around 1163, 1223, 1460, 1598, 1682 and 1828 cm^{-1} . The bands at 1163, 1223 and 1598 cm^{-1} were assigned to NH_3 coordinated to Lewis acid sites (Larrubia et al., 2005;

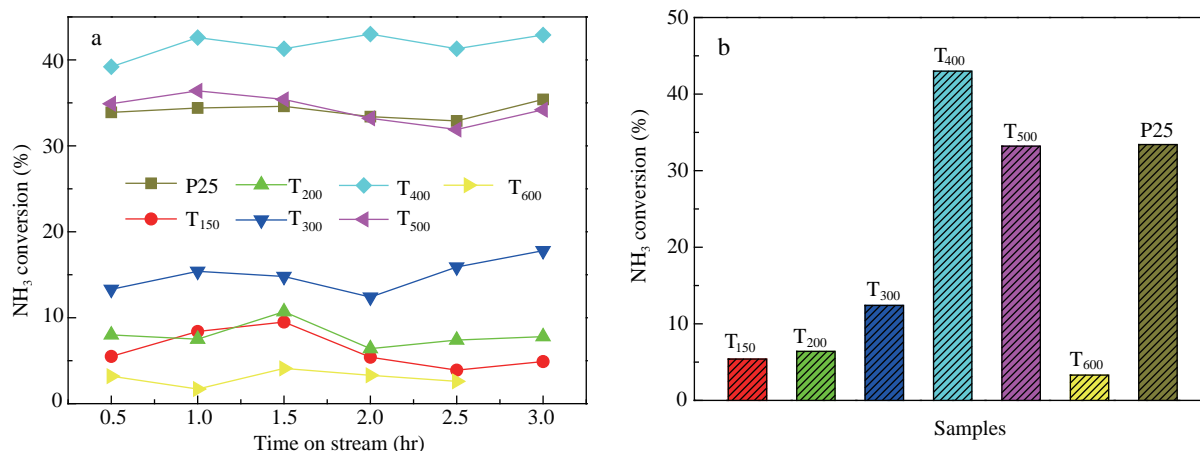


Fig. 8 (a) Activities of the catalysts calcined at different temperatures for the PCO of NH_3 as a function of UV light irradiation time and (b) NH_3 conversion after 2 hr reaction over catalysts calcined at different temperatures.

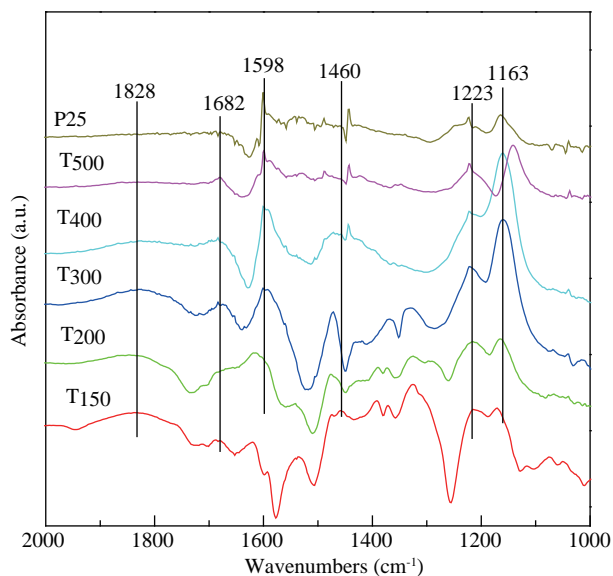


Fig. 9 *In situ* DRIFTS results of NH_3 adsorption over the TiO_2 samples prepared at various temperatures.

Liu and He, 2010) and the bands at around 1460 and 1682 cm^{-1} were assigned to NH_4^+ coordinated to Brønsted acid sites (Topsoe, 1994; Liu and He, 2010). The peak at 1828 cm^{-1} was due to physisorbed NH_3 . From the comparison among the spectra, we can see that the calcination temperature demonstrated a significant influence on the NH_3 adsorption. The T_{150} sample only presented a physisorbed NH_3 peak and no clear chemically-adsorbed NH_3 peaks appeared. The T_{200} sample showed very weak chemical NH_3 adsorption peaks at 1163, 1223, 1460 and 1598 cm^{-1} alongside the physisorbed NH_3 peak at 1828 cm^{-1} . Increasing the calcination temperature to 300 and 400°C gradually suppressed the physical NH_3 adsorption, but dramatically improved the chemical NH_3 adsorption on both the Lewis acid and Brønsted acid sites. The T_{400} sample presented the largest NH_3 adsorption peaks among the series of catalysts, especially the adsorption peaks over the Brønsted acid sites at around 1460 cm^{-1} . Further increasing the temperature to 500°C resulted in a decrease of chemical NH_3 adsorption possibly due to the decrease of the SSA. In addition, the commercial P25 showed a similar spectrum to that of the T_{500} sample. These results show that the samples calcined in the low temperature range ($<300^\circ\text{C}$) contained a very low amount of acid sites on the surface, which could be due to covering of the sites by residual carbon species. Increasing the calcination temperature reduces the carbon contents and then exposes the acid sites for the NH_3 adsorption and activation.

3 Conclusions

In situ DRIFTS results of NH_3 desorption combined with the activity test results revealed that the activities of

samples prepared at various temperatures for PCO of NH_3 were closely related to the surface acidity, and especially to the amount of Brønsted acid sites. The T_{200} sample had very high SSA, good crystallinity, strong visible light absorption, and also low PL intensity. However, this catalyst had few acid sites for NH_3 adsorption and activation, therefore showing no visible light activity for the PCO of NH_3 . The T_{400} sample had moderate SSA, the widest band gap and also high PL intensity, but this sample possessed the highest number of acid sites, therefore demonstrating the highest NH_3 removal performance under UV light among the series of catalysts.

In summary, the calcination temperature had a large effect on the PCO of NH_3 by changing the SSA, crystallinity, carbon residuals, band gap, PL emission and also the surface acidity of the TiO_2 . The carbon residuals account for their visible light adsorption and low band gap. However, the surface acidity plays a determining role in the PCO of NH_3 under both visible and UV light. The T_{200} sample, with its very low band gap and low PL intensity, showed very low visible and UV light activity for NH_3 oxidation due to its very low number of acid sites. The T_{400} sample, which had the highest number of acid sites, exhibited the highest NH_3 removal performance under UV light, even better than the commercial P25.

Acknowledgments

This work was supported by the National Natural Science Foundation of China (No. 21077117), the Strategic Priority Research Program of the Chinese Academy of Sciences (No. XDB05050600), and the Program of the Ministry of Science and Technology of China (No. 2010AA064905).

REFERENCES

- Akah, A., Cundy, C., Garforth, A., 2005. The selective catalytic oxidation of NH_3 over Fe-ZSM-5. *Appl. Catal. B* 59(3-4), 221–226.
- Bai, Z.P., Dong, Y.C., Wang, Z., Zhu, T., 2006. Emission of ammonia from indoor concrete wall and assessment of human exposure. *Environ. Int.* 32(3), 303–311.
- Balachandran, U., Erer, N.G., 1982. Raman spectra of titanium dioxide. *J. Solid State Chem.* 42(3), 276–282.
- Carp, O., 2004. Photoinduced reactivity of titanium dioxide. *Prog. Solid State Chem.* 32(1-2), 33–177.
- Chen, F.N., Yang, X.D., Wu, Q., 2009. Photocatalytic oxidation of *Escherichia coli*, *Aspergillus niger*, and formaldehyde under different ultraviolet irradiation conditions. *Environ. Sci. Technol.* 43(12), 4606–4611.
- Chen, X.B., Mao, S.S., 2007. Titanium dioxide nanomaterials: Synthesis, properties, modifications, and applications. *Chem. Rev.* 107(7), 2891–2959.
- Chen, X.F., Wang, X.C., Hou, Y.D., Huang, J.H., Wu, L., Fu, X.Z., 2008. The effect of postnitridation annealing on the surface property and photocatalytic performance of N-doped TiO_2 under visible light irradiation. *J. Catal.* 255(1), 59–67.
- Cheng, X.W., Yu, X.J., Xing, Z.P., 2012. Characterization and mechanism

- analysis of N doped TiO₂ with visible light response and its enhanced visible activity. *Appl. Surf. Sci.* 258(7), 3244–3248.
- Choi, H.J., Kim, J.S., Kang M., 2007. Photodecomposition of concentrated ammonia over nanometer-sized TiO₂, V-TiO₂, and Pt/V-TiO₂ photocatalysts. *Bull. Korean Chem. Soc.* 28(4): 581–588.
- Cui, X.Z., Zhou, J., Ye, Z.Q., Chen, H.R., Li, L., Ruan, M.L. et al. 2010. Selective catalytic oxidation of ammonia to nitrogen over mesoporous CuO/RuO₂ synthesized by co-nanocasting-replication method. *J. Catal.* 270(2), 310–317.
- Dong, F., Guo, S., Wang, H.Q., Li, X.F., Wu, Z.B., 2011. Enhancement of the visible light photocatalytic activity of C-doped TiO₂ nanomaterials prepared by a green synthetic approach. *The J. Phys. Chem. C* 115(27), 13285–13292.
- Dong, F., Wang, H.Q., Wu, Z.B., 2009. One-step “Green” synthetic approach for mesoporous C-doped titanium dioxide with efficient visible light photocatalytic activity. *The J. Phys. Chem. C* 113(38), 16717–16723.
- Dong, Y.C., Bai, Z.P., Liu, R.H., Zhu, T., 2007a. Decomposition of indoor ammonia with TiO₂-loaded cotton woven fabrics prepared by different textile finishing methods. *Atmos. Environ.* 41(15), 3182–3192.
- Dong, Y.C., Bai, Z.P., Liu, R.H., Zhu, T., 2007b. Preparation of fibrous TiO₂ photocatalyst and its optimization towards the decomposition of indoor ammonia under illumination. *Catal. Today* 126(3–4), 320–327.
- Fischer, M.L., Littlejohn, D., Lunden, M.M., Brown, N.J., 2003. Automated measurements of ammonia and nitric acid in indoor and outdoor air. *Environ. Sci. Technol.* 37(10), 2114–2119.
- Fu, J., Ji, M., An, D.N., 2005. Fulvic acid degradation using nanoparticle TiO₂ in a submerged membrane photocatalysis reactor. *J. Environ. Sci.* 17(6), 942–945.
- Górska, P., Zaleska, A., Kowalska, E., Klimczuk, T., Sobczak, J.W., Skwarek, E. et al., 2008. TiO₂ photoactivity in vis and UV light: The influence of calcination temperature and surface properties. *Appl. Catal.* 84(3), 440–447.
- Geng, Q.J., Guo, Q.J., Cao, C.Q., Zhang, Y.C., Wang, L.T., 2008a. Investigation into photocatalytic degradation of gaseous ammonia in CPCR. *Indust. Engine. Chem. Res.* 47(13), 4363–4368.
- Geng, Q.J., Wang, X.K., Tang, S.F., 2008b. Heterogeneous photocatalytic degradation kinetic of gaseous ammonia over nano-TiO₂ supported on latex paint film. *Biom. Environ. Sci.* 21(2), 118–123.
- Guo, T., Bai, Z.P., Wu, C., Zhu, T., 2008. Influence of relative humidity on the photocatalytic oxidation (PCO) of toluene by TiO₂ loaded on activated carbon fibers: PCO rate and intermediates accumulation. *Appl. Catal.* 79(2), 171–178.
- He, Z.L., Zhu, Z.F., Li, J.Q., Zhou, J.Q., Wei, N., 2011. Characterization and activity of mesoporous titanium dioxide beads with high surface areas and controllable pore sizes. *J. Hazard. Mater.* 190(1–3), 133–139.
- Hoffmann, M.R., Martin, S.T., Choi, W., Bahnemann, D.W., 1995. Environmental applications of semiconductor photocatalysis. *Chem. Rev.* 95(1), 69–96.
- Hou, H.M., Miyafuji, H., Kawamoto, H., Saka, S., 2006. Supercritically treated TiO₂-activated carbon composites for cleaning ammonia. *J. Wood Sci.* 52(6), 533–538.
- Huang, Y., Ho, W., Lee, S., Zhang, L., Li, G., Jimmy, C.Y., 2008. Effect of carbon doping on the mesoporous structure of nanocrystalline titanium dioxide and its solar-light-driven photocatalytic degradation of NO_x. *Langmuir* 24(7), 3510–3516.
- In, S., Orlov, A., Berg, R., Garca, F., Pedrosa-Jimenez, S., Tikhov, M.S. et al., 2007. Effective visible light-activated B-doped and B, N-codoped TiO₂ photocatalysts. *J. Amer. Chem. Soc.* 129(45), 13790–13791.
- Jimmy, C.Y., Ho, W., Yu, J., Yip, H., Wong, P.K., Zhao, J., 2005. Efficient visible-light-induced photocatalytic disinfection on sulfur-doped nanocrystalline titania. *Environ. Sci. Technol.* 39(4), 1175–1179.
- Kang, I.C., Zhang, Q., Yin, S., Sato, T., Saito, F., 2008. Improvement in photocatalytic activity of TiO₂ under visible irradiation through addition of N-TiO₂. *Environ. Sci. Technol.* 42(10), 3622–3626.
- Kim, K., Shin, C., 2001. Adsorption of ammonia on the sulfuric acid treated ACF. *Carbon Sci.* 2(2), 109–112.
- Kolinko, P.A., Kozlov, D.V., 2009. Products distribution during the gas phase photocatalytic oxidation of ammonia over the various titania based photocatalysts. *Appl. Catal. B* 90(1–2), 126–131.
- Kuo, C.S., Tseng, Y.H., Huang, C.H., Li, Y.Y., 2007. Carbon-containing nano-titania prepared by chemical vapor deposition and its visible-light-responsive photocatalytic activity. *J. Mol. Catal. A* 270(1), 93–100.
- Kuroda, Y., Mori, T., Yagi, K., Makihata, N., Kawahara, Y., Nagao, M. et al., 2005. Preparation of visible-light-responsive TiO₂-xNx photocatalyst by a sol-gel method analysis of the active center on TiO₂ that reacts with NH₃. *Langmuir* 21, 8026–8034.
- Larrubia, M.A., Arrighi, L., Ramis, G., 2005. Catalytic abatement of NO_x: Chemical and mechanistic aspects. *Catal. Today* 107, 139–148.
- Leary, R., Westwood, A., 2011. Carbonaceous nanomaterials for the enhancement of TiO₂ photocatalysis. *Carbon* 49(3), 741–772.
- Lettmann, C., Hildenbrand, K., Kisch, H., Macyk, W., Maier, W.F., 2001. Visible light photodegradation of 4-chlorophenol with a coke-containing titanium dioxide photocatalyst. *Appl. Catal.* 32(4), 215–227.
- Li, H.X., Zhang, X.Y., Huo, Y.N., Zhu, J., 2007. Supercritical preparation of a highly active S-doped TiO₂ photocatalyst for methylene blue mineralization. *Environ. Sci. Technol.* 41(12), 4410–4414.
- Li, Q., Shang, J.K., 2010. Composite photocatalyst of nitrogen and fluorine codoped titanium oxide nanotube arrays with dispersed palladium oxide nanoparticles for enhanced visible light photocatalytic performance. *Environ. Sci. Technol.* 44(9), 3493–3499.
- Li, Y.J., Chen, J., Liu, J.B., Ma, M.Y., Chen, W., Li, L.Y., 2010. Activated carbon supported TiO₂-photocatalysis doped with Fe ions for continuous treatment of dye wastewater in a dynamic reactor. *J. Environ. Sci.* 22(8), 1290–1296.
- Lin, Y.M., Tseng, Y.H., Huang, J.H., Chao, C.C., Chen, C.C., Wang, I., 2006. Photocatalytic activity for degradation of nitrogen oxides over visible light responsive titania-based photocatalysts. *Environ. Sci. Technol.* 40(5), 1616–1621.
- Liu, F.D., He, H., 2010. Structure-activity relationship of iron titanate catalysts in the selective catalytic reduction of NO_x with NH₃. *J. Phys. Chem.* 114(40), 16929–16936.
- Liu, Y., Yu, H.B., Lü, Z.N., Zhan, S.H., Yang, J.Y., Peng, X.H. et al., 2012. Simulated-sunlight-activated photocatalysis of Methylene Blue using cerium-doped SiO₂/TiO₂ nanostructured fibers. *J. Environ. Sci.* 24(10), 1867–1875.
- Lü, K.L., Hu, J.C., Li, X.H., Li, M., 2012. Cysteine modified anatase TiO₂ hollow microspheres with enhanced visible-light-driven photocatalytic activity. *J. Mol. Catal. A* 356, 78–84.

- Macwan, D.P., Dave, P.N., Chaturvedi, S., 2011. A review on nano-TiO₂ sol-gel type syntheses and its applications. *J. Mater. Sci.* 46(11), 3669–3686.
- Meng, Z.Y., Lin, W.L., Jiang, X.M., Yan, P., Wang, Y., Zhang, Y.M. et al., 2011. Characteristics of atmospheric ammonia over Beijing, China. *Atmos. Chem. Phys.* 11(12), 6139–6151.
- Miyawaki, J., Shimohara, T., Shirahama, N., Yasutake, A., Yoshikawa, M., Mochida, I. et al., 2011. Removal of NO_x from air through cooperation of the TiO₂ photocatalyst and urea on activated carbon fiber at room temperature. *Appl. Catal. B*, 110, 273–278.
- Mo, J., Zhang, Y., Xu, Q., Lamson J.J., Zhao R., 2009. Photocatalytic purification of volatile organic compounds in indoor air: A literature review. *Atmos. Environ.* 43(14), 2229–2246.
- Nazir, M., Takasaki, J., Kumazawa, H., 2003. Photocatalytic degradation of gaseous ammonia and trichloroethylene over TiO₂ ultrafine powders deposited on activated carbon particles. *Chem. Eng. Commun.* 190(3), 322–333.
- Porter J.F., Li, Y.G., Chan, C.K., 1999. The effect of calcination on the microstructural characteristics and photoreactivity of Degussa P25 TiO₂. *J. Mater. Sci.* 34(7), 1523–1531.
- Ren, W.J., Ai, Z.H., Jia, F.L., Zhang, L.Z., Fan, X.X., Zou, Z.G., 2007. Low temperature preparation and visible light photocatalytic activity of mesoporous carbon-doped crystalline TiO₂. *Appl. Catal. B* 69(3), 138–144.
- Shen, M., Wu, Z.Y., Huang, H., Du, Y.K., Zou, Z.G., Yang, P., 2006. Carbon-doped anatase TiO₂ obtained from TiC for photocatalysis under visible light irradiation. *Mater. Lett.* 60(5), 693–697.
- Shi, J.Y., Chen, J., Feng, Z.C., Chen, T., Lian, Y.X., Wang, X.L. et al., 2007. Photoluminescence characteristics of TiO₂ and their relationship to the photoassisted reaction of water/methanol mixture. *J. Phys. Chem. C* 111(2), 693–699.
- Tojo, S., Tachikawa, T., Fujitsuka, M., Majima, T., 2008. Iodine-doped TiO₂ photocatalysts: correlation between band structure and mechanism. *J. Phys. Chem. C* 112(38), 14948–14954.
- Topsoe, N.Y., 1994. Mechanism of the selective catalytic reduction of nitric-oxide by ammonia elucidated by *in-situ* online Fourier-transform infrared-spectroscopy. *Science* 265(5176), 1217–1219.
- Tseng, Y.H., Kuo, C.S., Huang, C.H., Li, Y.Y., Chou, P.W., Cheng, C.L. et al., 2006. Visible-light-responsive nano-TiO₂ with mixed crystal lattice and its photocatalytic activity. *Nanotechnology* 17(10), 2490–2497.
- Wang, G.H., Xu, L., Zhang, J., Yin, T.T., Han, D.Y., 2012. Enhanced photocatalytic activity of TiO₂ powders (P25) via calcination treatment. *Inter. J. Phot Article ID 265760*, 9, DOI: 10.1155/2012/265760.
- Wang, Q., Chen, C.C., Zhao, D., Ma, W.H., Zhao, J.C., 2008. Change of adsorption modes of dyes on fluorinated TiO₂ and its effect on photocatalytic degradation of dyes under visible irradiation. *Langmuir* 24(14), 7338–7345.
- Xiao, Q., Ouyang, L., 2009. Photocatalytic activity and hydroxyl radical formation of carbon-doped TiO₂ nanocrystalline: Effect of calcination temperature. *Chem. Eng. J.* 148(2), 248–253.
- Xue, X.X., Ji, W., Mao, Z., Mao, H. J., Wang, Y., Wang, X., et al., 2012. Raman investigation of nanosized TiO₂: Effect of crystallite size and quantum confinement. *J. Phys. Chem. C* 116(15), 8792–8797.
- Yamazoe, S., Okumura, T., Hitomi, Y., Shishido, T., Tanaka, T., 2007a. Mechanism of photo-oxidation of NH₃ over TiO₂: Fourier transform infrared study of the intermediate species. *J. Phys. Chem. C* 111(29), 11077–11085.
- Yamazoe, S., Okumura, T., Tanaka, T., 2007b. Photo-oxidation of NH₃ over various TiO₂. *Catal. Today* 120(2), 220–225.
- Yu, J.C., Yu, J.U., Ho, W.K., Jiang, Z.T., Zhang, L.H., 2002. Effects of F-doping on the photocatalytic activity and microstructures of nanocrystalline TiO₂ powders. *Chem. Mater.* 14(9), 3808–3816.
- Yu, J.G., Ma, T.T., Liu, S.W., 2011. Enhanced photocatalytic activity of mesoporous TiO₂ aggregates by embedding carbon nanotubes as electron-transfer channel. *Phys. Chem. Chem. Phys.* 13(8), 3491–3501.
- Yu, J.G., Wang, G.H., Cheng, B., Zhou, M.H., 2007. Effects of hydrothermal temperature and time on the photocatalytic activity and microstructures of bimodal mesoporous TiO₂ powders. *Appl. Catal. B* 69(3–4), 171–180.
- Zhang, L., Zhang, C.B., He, H., 2009. The role of silver species on Ag/Al₂O₃ catalysts for the selective catalytic oxidation of ammonia to nitrogen. *J. Catal.* 261(1), 101–109.
- Zhang, Q.H., Gao, L., Guo, J.K., 2000. Effects of calcination on the photocatalytic properties of nanosized TiO₂ powders prepared by TiCl₄ hydrolysis. *Appl. Catal. B* 26(3), 207–215.



Editorial Board of Journal of Environmental Sciences

Editor-in-Chief

Hongxiao Tang Research Center for Eco-Environmental Sciences, Chinese Academy of Sciences, China

Associate Editors-in-Chief

Jiuhui Qu Research Center for Eco-Environmental Sciences, Chinese Academy of Sciences, China

Shu Tao Peking University, China

Nigel Bell Imperial College London, United Kingdom

Po-Keung Wong The Chinese University of Hong Kong, Hong Kong, China

Editorial Board

Aquatic environment

Baoyu Gao

Shandong University, China

Maohong Fan

University of Wyoming, USA

Chihpin Huang

National Chiao Tung University

Taiwan, China

Ng Wun Jern

Nanyang Environment &
Water Research Institute, Singapore

Clark C. K. Liu

University of Hawaii at Manoa, USA

Hokyong Shon

University of Technology, Sydney, Australia

Zijian Wang

Research Center for Eco-Environmental Sciences,
Chinese Academy of Sciences, China

Zhiwu Wang

The Ohio State University, USA

Yuxiang Wang

Queen's University, Canada

Min Yang

Research Center for Eco-Environmental Sciences,
Chinese Academy of Sciences, China

Zhifeng Yang

Beijing Normal University, China

Han-Qing Yu

University of Science & Technology of China

Terrestrial environment

Christopher Anderson

Massey University, New Zealand

Zucong Cai

Nanjing Normal University, China

Xinbin Feng

Institute of Geochemistry,
Chinese Academy of Sciences, China

Hongqing Hu

Huazhong Agricultural University, China

Kin-Che Lam

The Chinese University of Hong Kong
Hong Kong, China

Erwin Klumpp

Research Centre Juelich, Agrosphere Institute
Germany

Peijun Li

Institute of Applied Ecology,
Chinese Academy of Sciences, China

Michael Schloter

German Research Center for Environmental Health
Germany

Xuejun Wang

Peking University, China

Lizhong Zhu

Zhejiang University, China

Atmospheric environment

Jianmin Chen

Fudan University, China

Abdelwahid Mellouki

Centre National de la Recherche Scientifique
France

Yujing Mu

Research Center for Eco-Environmental Sciences,
Chinese Academy of Sciences, China

Min Shao

Peking University, China

James Jay Schauer

University of Wisconsin-Madison, USA

Yuesi Wang

Institute of Atmospheric Physics,
Chinese Academy of Sciences, China

Xin Yang

University of Cambridge, UK

Environmental biology

Yong Cai

Florida International University, USA

Henner Hollert

RWTH Aachen University, Germany

Jaе-Seong Lee

Hanyang University, South Korea

Christopher Rensing

University of Copenhagen, Denmark

Bojan Sedmak

National Institute of Biology, Ljubljana

Lirong Song

Institute of Hydrobiology,
the Chinese Academy of Sciences, China

Chunxia Wang

National Natural Science Foundation of China

Gehong Wei

Northwest A & F University, China

Daqiang Yin

Tongji University, China

Zhongtang Yu

The Ohio State University, USA

Environmental toxicology and health

Jingwen Chen

Dalian University of Technology, China

Jiaying Hu

Peking University, China

Guibin Jiang

Research Center for Eco-Environmental Sciences,
Chinese Academy of Sciences, China

Sijin Liu

Research Center for Eco-Environmental Sciences,
Chinese Academy of Sciences, China

Tsuyoshi Nakanishi

Gifu Pharmaceutical University, Japan

Willie Peijnenburg

University of Leiden, The Netherlands

Bingsheng Zhou

Institute of Hydrobiology,
Chinese Academy of Sciences, China

Environmental catalysis and materials

Hong He

Research Center for Eco-Environmental Sciences,
Chinese Academy of Sciences, China

Junhua Li

Tsinghua University, China

Wenfeng Shangguan

Shanghai Jiao Tong University, China

Yasutake Teraoka

Kyushu University, Japan

Ralph T. Yang

University of Michigan, USA

Environmental analysis and method

Zongwei Cai

Hong Kong Baptist University,
Hong Kong, China

Jiping Chen

Dalian Institute of Chemical Physics,
Chinese Academy of Sciences, China

Minghui Zheng

Research Center for Eco-Environmental Sciences,
Chinese Academy of Sciences, China

Municipal solid waste and green chemistry

Pinjing He

Tongji University, China

Environmental ecology

Rusong Wang

Research Center for Eco-Environmental Sciences,
Chinese Academy of Sciences, China

Editorial office staff

Managing editor Qingcai Feng

Editors Zixuan Wang Suqin Liu Zhengang Mao

English editor Catherine Rice (USA)

JOURNAL OF ENVIRONMENTAL SCIENCES

环境科学学报(英文版)
(<http://www.jesc.ac.cn>)

Aims and scope

Journal of Environmental Sciences is an international academic journal supervised by Research Center for Eco-Environmental Sciences, Chinese Academy of Sciences. The journal publishes original, peer-reviewed innovative research and valuable findings in environmental sciences. The types of articles published are research article, critical review, rapid communications, and special issues.

The scope of the journal embraces the treatment processes for natural groundwater, municipal, agricultural and industrial water and wastewaters; physical and chemical methods for limitation of pollutants emission into the atmospheric environment; chemical and biological and phytoremediation of contaminated soil; fate and transport of pollutants in environments; toxicological effects of terrorist chemical release on the natural environment and human health; development of environmental catalysts and materials.

For subscription to electronic edition

Elsevier is responsible for subscription of the journal. Please subscribe to the journal via <http://www.elsevier.com/locate/jes>.

For subscription to print edition

China: Please contact the customer service, Science Press, 16 Donghuangchenggen North Street, Beijing 100717, China. Tel: +86-10-64017032; E-mail: journal@mail.sciencep.com, or the local post office throughout China (domestic postcode: 2-580).

Outside China: Please order the journal from the Elsevier Customer Service Department at the Regional Sales Office nearest you.

Submission declaration

Submission of an article implies that the work described has not been published previously (except in the form of an abstract or as part of a published lecture or academic thesis), that it is not under consideration for publication elsewhere. The submission should be approved by all authors and tacitly or explicitly by the responsible authorities where the work was carried out. If the manuscript accepted, it will not be published elsewhere in the same form, in English or in any other language, including electronically without the written consent of the copyright-holder.

Submission declaration

Submission of the work described has not been published previously (except in the form of an abstract or as part of a published lecture or academic thesis), that it is not under consideration for publication elsewhere. The publication should be approved by all authors and tacitly or explicitly by the responsible authorities where the work was carried out. If the manuscript accepted, it will not be published elsewhere in the same form, in English or in any other language, including electronically without the written consent of the copyright-holder.

Editorial

Authors should submit manuscript online at <http://www.jesc.ac.cn>. In case of queries, please contact editorial office, Tel: +86-10-62920553, E-mail: jesc@263.net, jesc@rcees.ac.cn. Instruction to authors is available at <http://www.jesc.ac.cn>.

Journal of Environmental Sciences (Established in 1989)

Vol. 26 No. 3 2014

Supervised by	Chinese Academy of Sciences	Published by	Science Press, Beijing, China
Sponsored by	Research Center for Eco-Environmental Sciences, Chinese Academy of Sciences	Distributed by	Elsevier Limited, The Netherlands
Edited by	Editorial Office of Journal of Environmental Sciences P. O. Box 2871, Beijing 100085, China Tel: 86-10-62920553; http://www.jesc.ac.cn E-mail: jesc@263.net , jesc@rcees.ac.cn	Domestic	Science Press, 16 Donghuangchenggen North Street, Beijing 100717, China Local Post Offices through China
Editor-in-chief	Hongxiao Tang	Foreign	Elsevier Limited http://www.elsevier.com/locate/jes
CN 11-2629/X	Domestic postcode: 2-580	Printed by	Beijing Beilin Printing House, 100083, China
		Domestic price per issue	RMB ¥ 110.00

ISSN 1001-0742

